12-22-2020

ARP2/3-Independent WAVE/SCAR Pathway and Class XI Myosin Control Sperm Nuclear Migration in Flowering Plants

Mohammad F. Ali
University of Kentucky, M.Foteh.Ali@uky.edu

Umma Fatema
University of Kentucky, Umma.Fatema@uky.edu

Xiongbo Peng
Wuhan University, China

Samuel W. Hacker
University of Kentucky, samuel.hacker1@uky.edu

Daisuke Maruyama
Yokohama City University, Japan

See next page for additional authors

ARP2/3-Independent WAVE/SCAR Pathway and Class XI Myosin Control Sperm Nuclear Migration in Flowering Plants

Digital Object Identifier (DOI)
https://doi.org/10.1073/pnas.2015550117

Notes/Citation Information
Published in *PNAS*, v. 117, issue 51.

Authors
Mohammad F. Ali, Umma Fatema, Xiongbo Peng, Samuel W. Hacker, Daisuke Maruyama, Meng-Xiang Sun, and Tomokazu Kawashima

PNAS
www.pnas.org

Main Manuscript for

ARP2/3-Independent WAVE/SCAR Pathway and Class XI Myosin Control Sperm Nuclear Migration in Flowering Plants

Mohammad Foteh Ali[a], Umma Fatema[a], Xiongbo Peng[b], Samuel W. Hacker[c], Daisuke Maruyama[d], Mengxiang Sun[b], Tomokazu Kawashima[a,c,1]

[a]Department of Plant and Soil Sciences, University of Kentucky, Lexington, KY, 40546-0312

[b]State Key Laboratory of Hybrid Rice, College of Life Science, Wuhan University, Wuhan, 430072, China

[c]Agriculture and Medical Biotechnology Program, University of Kentucky, Lexington, KY, 40546-0312

[d]Kihara Institute for Biological Research, Yokohama City University, Yokohama, Kanagawa 244-0813, Japan

[1]To whom correspondence may be addressed. Email: tomo.k@uky.edu

https://orcid.org/0000-0003-3803-3070

Classification

Plant Biology

Keywords

gamete nuclear migration, F-actin, WAVE/SCAR, ARP2/3, myosin, fertilization

Author Contributions

MFA and TK conceived and designed the experiments. MFA performed Arabidopsis experiments and analyzed the data with the help of UF and SWH. XP and MS performed tobacco experiments. DM contributed resources critical to the experiments. MFA and TK wrote the paper. TK agrees to serve as the author responsible for contact and ensures communication.

This PDF file includes:

Main Text
Figures 1 to 5

Abstract

After eukaryotic fertilization, gamete nuclei migrate to fuse parental genomes in order to initiate development of the next generation. In most animals, microtubules control female and male pronuclear migration in the zygote. Flowering plants, on the other hand, have evolved actin filament (F-actin) based sperm nuclear migration systems for karyogamy. Flowering plants have also evolved a unique double fertilization process; two female gametophytic cells, the egg and central cells, are each fertilized by a sperm cell. The molecular and cellular mechanisms of how flowering plants utilize and control F-actin for double fertilization events are largely unknown. Using confocal microscopy live-cell imaging with a combination of pharmacological and genetic approaches, we identified factors involved in F-actin dynamics and sperm nuclear migration in *Arabidopsis thaliana* (Arabidopsis) and *Nicotiana tabacum* (tobacco). We demonstrate that the F-actin regulator, SCAR2, but not the ARP2/3 protein complex, controls the coordinated active F-actin movement. These results imply that a novel ARP2/3-independent WAVE/SCAR signaling pathway regulates F-actin dynamics in female gametophytic cells for fertilization. We also identify that the class XI myosin, XI-G, controls active F-actin movement in the Arabidopsis central cell. XI-G is not a simple transporter, moving cargos along F-actin, but can generate forces that control the dynamic movement of F-actin for fertilization. Our results provide new insights into the mechanisms that control gamete nuclear migration and reveal new regulatory pathways for dynamic F-actin movement in flowering plants.

Significance Statement

Flowering plants have evolved a unique double fertilization process along with an actin filament (F-actin) based gamete nuclear migration mechanism. However, how dynamic F-actin movement is controlled in the female gametophytic cells remains unclear. We identified that the movement of F-actin is promoted via a novel ARP2/3-independent WAVE/SCAR signalling pathway. We also discovered that plant class XI myosin, XI-G, has a new function involved in the active movement of F-actin required for sperm nuclear migration, which is different from the canonical myosin function as a cargo transporter. These breakthroughs also provide us with opportunities to further understand how flowering plants control double fertilization and plant cytoskeleton dynamics.

Main Text

Introduction

Flowering plants have evolved a unique double fertilization process. Two sperm cells fuse with two female gametophytic cells, the egg and central cells within the ovule (Fig. 1*A*), giving rise to the embryo and endosperm, respectively (1, 2). Sperm cells in flowering plants are non-motile and delivered in close proximity to the egg and central cells by the pollen tube. After gamete cell fusion, in most animals, both

male and female pronuclei move toward each other within the fertilized egg for gamete nuclear fusion, or karyogamy. Pronuclei movement is regulated by microtubules that assemble the sperm aster from the centrosome (3, 4). By contrast, flowering plants have lost the centrosome, and have established actin filament (F-actin) based sperm nuclear migration systems for successful double fertilization (5–7). Prior to fertilization, both the egg and central cells form a mesh-like structure of F-actin that shows constant inward movement from the plasma membrane to the center of the cell, where the nucleus resides (Fig. 1*A*) (5, 8, 9). This meshwork movement begins prior to gamete cell fusion and continues until the completion of karyogamy (5). In *Arabidopsis thaliana* (Arabidopsis) and *Oryza sativa* (rice), F-actin aster-like structures are formed surrounding the sperm nuclei just after the sperm nuclei enter into the female gametophytic cells. The transfer of the actin aster-sperm nucleus complex coincides with the constant F-actin meshwork movement (5, 9). The movement of the sperm nucleus by F-actin is consistent in *Nicotiana tabacum* (tobacco) and *Zea mays* (maize), and disruption of F-actin arrests sperm nuclear migration (5–7). These results demonstrate that coordinated F-actin meshwork inward movement plays an essential role in sperm nuclear migration of flowering plants.

F-actin meshwork movement in the female gametophytic cell requires the constant formation of F-actin at the plasma membrane. The rate of F-actin formation can be controlled by regulators that nucleate actin monomers to initiate new filaments, control polymerization during elongation, and prevent disassembly of F-actin (10). In plants, membrane-associating small GTPase signaling proteins, Rho-GTPase of Plants (ROPs), facilitate cell morphogenesis by controlling actin polymerization (11, 12). The Wiskott–Aldrich syndrome protein family verprolin-homologous/suppressor of cAMP receptor (WAVE/SCAR) family are effector proteins that directly interact with ROPs and promote actin nucleation (13, 14). The WAVE/SCAR complex is the main activator of the F-actin regulatory ACTIN RELATED PROTEIN 2/3 (ARP2/3) protein complex (15, 16). ARP2/3 directly promotes polymerization of branched actin filaments from the sides of preexisting actin filaments and forms a highly dense branched F-actin network (17, 18). Phenotypes of functionally null single or combinatorial mutants of any of these WAVE/SCAR-ARP2/3 components have been intensively studied in trichomes (15, 19–21), and the lack of intermediate phenotypes indicates that the WAVE/SCAR and ARP2/3 protein complexes constitute the sole pathway that controls the trichome morphology via F-actin regulation (14, 19). The involvement of WAVE/SCAR in sperm nuclear migration has been suggested in the egg and central cells of tobacco and maize using wiskostatin, an inhibitor for WAVE/SCAR activity (7). However, it still remained open whether the WAVE/SCAR activity is mediated through the ARP2/3 pathway, and the genetic data confirming the role of WAVE/SCAR-ARP2/3 in fertilization were still missing.

The Arabidopsis central cell is more than five times larger than the egg cell. This large cell size allows us to visualize F-actin dynamics in detail (4, 5), thus providing an excellent platform to understand the dynamics of plant fertilization. *ROP8* is specifically expressed in the central cell and promotes the assembly of F-actin at the plasma membrane, maintaining the constant F-actin meshwork movement (5).

Several pharmacological analyses identified putative factors, such as the F-actin motor proteins, myosins, that can control the dynamic F-actin meshwork movement in the female gametophytic cells (5, 7, 9). However, apart from the genetically confirmed *ROP8* involvement in the Arabidopsis central cell, it remained largely unknown how F-actin movement for sperm nuclear migration is regulated (5). To identify what factors and pathways are involved in F-actin movement for sperm nuclear migration in flowering plants, we performed genetic and pharmacological analyses with live-cell confocal microscopy imaging in Arabidopsis. We show that WAVE/SCAR and class XI myosin, but not the ARP2/3 complex, play important roles in sperm nuclear migration. New insights into the novel ARP2/3-independent WAVE/SCAR pathway as well as the newly discovered role of class XI myosin in the female gametophyte will facilitate further understanding of the mechanism of plant fertilization and cytoskeleton dynamics in flowering plants.

Results

F-actin meshwork movement in the female gametophytic cell is SCAR2 dependent, but ARP2/3 independent.

F-actin meshwork in the Arabidopsis central cell is initiated at the plasma membrane by ROP8 and moves to the nucleus for sperm nuclear migration (5). In plants, ROPs promote F-actin nucleation by interacting with WAVE/SCAR (13, 14). To investigate the involvement of WAVE/SCAR, we applied wiskostatin (22), a small molecule that inhibits WAVE/SCAR activity, to dissected Arabidopsis ovules and examined F-actin meshwork movement in the central cell. Wiskostatin stabilizes the native auto-inhibitory interaction between the GTPase-binding domain (GBD) and the VCA (verprolin homology) domain of WAVE/SCAR proteins (22, 23). The movement of the central cell F-actin meshwork in the F-actin marker line (*proFWA::lifeact:Venus*) (5) was impaired when treated with 10 µM wiskostatin (Fig. 1 *B, C,* and *H* and *SI Appendix*, Movie S1), suggesting that the WAVE/SCAR activity is required for F-actin dynamics in the central cell.

Among Arabidopsis *SCARs*, *SCAR2* and *SCAR4* appear to be expressed in the central cell with *SCAR2* expression being higher (24, 25). We observed sperm nuclear migration phenotypes in the wild-type (WT), *scar2-1* (26)*, scar4-1* (13), and *scar2-1;4-1* double mutant plants by pollinating them with the sperm-specific histone marker line (*proHTR10::HTR10:mRFP1*) (Fig. 2 and *SI Appendix*, Fig. S1) (27). After sperm release to the ovule (Fig. 2*A*), sperm nuclei, containing condensed chromatin, start migrating toward the nucleus of the egg and central cells (Fig. 2*B*). Sperm nuclear migration is a rapid event that is completed within five minutes (5), then followed by karyogamy and sperm chromatin decondensation (Fig. 2*C*). Sperm chromatin decondensation only starts after successful karyogamy (5, 28, 29). In *scar2-1* and *scar2-1;4-1,* 33.9 and 35.8 % of ovules showed no or partially decondensed sperm chromatin in the central cell, respectively (Fig. 2 *D*, *E,* and *SI Appendix*, Fig. S1). We did not observe this decondensation-delay phenotype in either WT or *scar4-1* (Fig. 2*E*). Consistently, the central cell F-actin meshwork movement in

scar2-1 and *scar2-1;4-1* were significantly slower than that of WT or *scar4-1* (Fig. 1 B, *D*, *H; SI Appendix*, Fig. S2 and Movie S1). These results show that *SCAR2* is the main SCAR factor that controls the central cell F-actin meshwork movement important for sperm nuclear migration.

The activation of the ARP2/3 complex through the WAVE/SCAR pathway is required to induce cellular actin nucleation (14–16). To investigate the involvement of the ARP2/3 complex, the effect of an ARP2/3 complex inhibitor, CK-666 (30), on the central cell F-actin meshwork movement was examined. CK-666 (40-200 µM) stabilizes the inactive state of the complex, blocking the movement of the ARP2 and ARP3 subunits into the activated filament-like conformation (30, 31). 200 µM CK-666 application altered the F-actin orientation to perpendicular to the long axis of the cell in the cotyledon pavement cell (*SI Appendix*, Fig. S3 *A* and *B*), which is typical of ARP2/3 mutants (*SI Appendix,* Fig. S4) (20). Surprisingly, 200 µM CK-666 did not affect F-actin meshwork movement in the central cell even after one-hour incubation (Fig. 1 *B*, *F* and *H* and *SI Appendix*, Movie S1). These results suggest that the ARP2/3 complex is not involved in F-actin meshwork movement in the central cell. To genetically confirm that ARP2/3 is dispensable for sperm nuclear migration, we investigated the fertilization phenotype in the *arp2-1* (20), *dis2-1 (arpc2)* (32), and *arpc4-t2* (33) mutants. None of these mutants showed significant difference in either F-actin meshwork movement (Fig. 1 *B, G, H; SI Appendix*, Fig. S2 and Movie S1) or sperm nuclear migration (Fig. 2*E*, and *SI Appendix*, Fig. S1) compared to WT. Gene expression data indicate that *ARP2* is expressed in the central cell (24, 25), and indeed, the *ARP2* promoter activated expression in the central cell (Fig. 1*E*). These results show that, although *ARP2* is expressed in the central cell, ARP2/3 is not involved in fertilization, and provide genetic evidence that *SCAR2* regulates F-actin dynamics in the central cell through a novel ARP2/3-independent pathway.

The class XI myosin, XI-G, plays a major role in the active movement of F-actin meshwork in the female gametophytic cell for fertilization.

2, 3-butanedione monoxime (BDM) inhibits myosin activity by blocking an ATPase activity of the myosin superfamily (5, 7, 9). The application of BDM to Arabidopsis ovules arrests F-actin meshwork movement (5), indicative of myosin involvement. The class XI myosin gene, *XI-G*, shows relatively high expression compared to other class XI myosins in the Arabidopsis central cell (25, 24), and the *XI-G* promoter activated transcription in the central cell and synergid cells of the female gametophyte (Fig. 3*E*). The *xi-g* knockout mutant (34) displayed significantly slower F-actin meshwork movement in the central cell compared to WT (Fig. 3 *A, B,* and *F* and *SI Appendix*, Movie S2). Similar to *scar2-1* (Fig. 2*E*), 40% of *xi-g* ovules had no or partially decondensed sperm chromatin in the central cell (Fig. 2*E*, and *SI Appendix*, Fig. S1). These data genetically show that the class XI myosin XI-G plays a major role in F-actin dynamics for sperm nuclear migration in the central cell.

F-actin meshwork movement is controlled by a non-canonical function of the myosin.

The application of 20 mM BDM did not cause any change in F-actin meshwork movement (Fig. 3 *A, C,* and *F,* and *SI Appendix*, Movie S2); however, 50 mM BDM application immediately stopped F-actin meshwork movement (Fig. 3 *A, D,* and *F* and *SI Appendix*, Movie S2). Myosin XI generates the power for filament buckling and straightening by sliding antiparallel actin filaments and/or translocating actin filaments along membranes (35, 36). We also checked F-actin structures in the presence of BDM and we observed that actin filaments were straightened and parallel with each other in 50 mM BDM, but not in a 20 mM treatment (Fig. 3 *A, C, D, G, SI Appendix*, Fig. S5 and Movie S2). These data further support that 50 mM BDM is required for the clear observation of myosin inhibitory function in F-actin meshwork movement in the Arabidopsis central cell.

In contrast to the lack of effect on F-actin meshwork movement with 20 mM BDM in the central cell (Fig. 3 *A, C,* and *F* and *SI Appendix*, Movie S2), 20 mM or less BDM can inhibit the myosin function as a cargo transporter in tobacco leaf and maize root apex cells (7, 37). To investigate the effect of BDM on organelle movement in the Arabidopsis central cell, we monitored mitochondrial dynamics using the Arabidopsis central-cell mitochondrial marker line *proDD65::coxIV:GFP* (38). Mitochondrial motility in the central cell was reduced immediately with 20 mM BDM application compared to the mock (Fig. 4 and *SI Appendix*, Movie S3). At 20 mM, BDM does not affect F-actin meshwork movement (Fig. 3*F*), showing that F-actin meshwork moves without organelle movement in the central cell. We also found that mitochondrial motility was not affected in either the *xi-g*, *scar2-1,* or *arp2-1* central cell (Fig. 4, *SI Appendix*, Fig. S6 and Movie S3). The central cell F-actin meshwork movements in *xi-g* and *scar2-1* are greatly reduced (Figs. 1*H* and 3*F*). Taken together, these results indicate that F-actin meshwork movement in the central cell is independent of organelle movement and that XI-G controls F-actin meshwork movement through a non-cargo transport function of the myosin.

F-actin meshwork movement controlled by myosin is conserved across the plant kingdom.

In tobacco, as low as 2 mM BDM application stops mitochondrial movement in leaf cells (7). On the other hand, like in Arabidopsis (Fig. 3 *A, C,* and *F* and *SI Appendix*, Movie S2), 20 mM BDM does not impair sperm nuclear migration in the tobacco central cell (7). To verify the involvement of myosins in sperm nuclear migration in tobacco, 50 mM BDM was applied to tobacco central cells and sperm nuclear migration was monitored. Sperm nuclei incorporated into tobacco central cells dissected out from the ovule did not move toward the polar nuclei with 50 mM BDM (*SI Appendix*, Fig. S7 and Movie S4). These results show that the active role of myosins in F-actin meshwork movement for sperm nuclear migration is conserved among flowering plants. Furthermore, the differences in the BDM sensitivity between mitochondrial movement and F-actin meshwork movement in both Arabidopsis (Figs. 3*C* and 4*B*) and tobacco central cells (*SI Appendix*, Fig. S7 and Movie S4) (7) show that the myosin function for F-actin meshwork movement is distinct from the canonical organelle transport function.

Discussion

In flowering plants, F-actin controls sperm nuclear migration for successful fertilization. This work has revealed that novel F-actin regulatory pathways involving class XI myosin XI-G (Fig. 3 *B* and *F*), SCAR2 (Fig. 1*H*), but not the ARP2/3 complex (Fig. 1*H* and *SI Appendix*, Fig. S2*F*), regulate F-actin dynamics in the female gametophytic cell that are important for sperm nuclear migration. In trichomes and cotyledon pavement cells, WAVE/SCAR solely relays the signal to ARP2/3 for F-actin organization (15, 16, 19). Our results indicate that a novel ARP2/3-independent WAVE/SCAR F-actin regulatory pathway exists in the Arabidopsis female gametophytic cell (Fig. 5). We also revealed that the plant-specific class XI myosin, *XI-G,* is critical for F-actin meshwork movement required for sperm nuclear migration in the Arabidopsis central cell. Class XI myosins are known to control the organization of F-actin and generate force for filament buckling and straightening in somatic cells (36, 39). However, the movement of F-actin from the plasma membrane to the nucleus in the female gametophytic cell occurs at the whole-cell level, and the involvement of XI-G on such a large-scale as occurs in the dynamic F-actin inward movement is novel. Furthermore, this newly identified myosin function is distinct from the myosin canonical function as the organelle transporter (Figs. 3 and 4).

The plant Rho-GTPase gene, *ROP8*, and *SCAR2* are both expressed in the Arabidopsis central cell (5, 24, 25), and they directly interact with each other (13). The mutants show both reduced F-actin meshwork inward movement (Fig. 1 *D* and *H*) (5) and delay in sperm nuclear migration (Fig. 2*E* and *SI Appendix*, Fig. S1) (5), indicating that a ROP8-SCAR2 mediated signaling pathway controls F-actin dynamics in the Arabidopsis central cell (Fig. 5). In SCARs, besides highly conserved SHD and WA domains, there are plant-specific domains with unknown functions (14). It is possible that these domains control the ARP2/3-independent WAVE/SCAR pathway in the female gametophytic cell for fertilization. Functional domain dissections of SCAR2 and the identification of other WAVE/SCAR pathway genes' (15, 40–42) involvement will be awaited to further understand this novel ARP2/3-independent WAVE/SCAR pathway in the female gametophyte. *SCAR4* is also expressed in the central cell (24, 25, 43). However, fertilization is not affected in *scar4-1* (Fig. 2*E* and *SI Appendix*, Fig. S2*F*) and the *scar2-1;4-1* double mutant shows neither additive nor synergistic effects (*SI Appendix*, Fig. S2*F*). These results indicate that the *SCAR4* pathway is distinct from the *SCAR2* pathway in the central cell. Similar to *SCAR4*, *ARP2* is also expressed in the central cell (Fig. 1*E*) and is dispensable for proper F-actin meshwork movement (Figs. 1*H* and 2*E*). *SCAR4* may play a role in the canonical WAVE/SCAR-ARP2/3 pathway, possibly controlling F-actin branching in the central cell for processes other than gamete nuclear migration.

Our myosin studies (Figs. 3 and 4) indicate that the myosin-driven organelle movement does not play a role in F-actin meshwork movement and there must exist a different mechanism by which XI-G controls F-actin meshwork movement in the Arabidopsis central cell. *In vitro,* myosins can cross-link actin filaments and myosin motor activity generates contractile forces that result in directional F-actin movement (44, 45). These F-actin dynamics are similar to F-actin meshwork inward movement observed in the female gametophytic cell (5, 9). Any mutants displaying a defect of F-actin meshwork movement do not completely

arrest sperm nuclear migration in the central cell (Fig. 2*E*). Therefore, in parallel to *SCAR2,* other pathways such as class XI myosins and/or other actin nucleators such as formins (46) likely control F-actin meshwork movement. In the case of class XI myosins, gene functional redundancy (47) may partially complement the XI-G function for maintaining F-actin meshwork in the central cell. XI-I interacts with the nucleus, linking the nuclear envelope with F-actin to maintain the position and shape of the nucleus; however, unlike XI-G, XI-I itself does not regulate F-actin movement (48). Although *XI-I* appears to be less expressed in the female gametophytic cells including the central cell (24, 25), XI-I may help the incorporated sperm nucleus associate rapidly with F-actin meshwork in the female gametophytic cells for fertilization. Further analyses will reveal how class XI myosins play their roles in the unique F-actin dynamics in the central cell.

In flowering plants, the double fertilization events of the egg and central cells are regulated independently, but the essential role of F-actin in sperm nuclear migration is conserved in both cells (5, 7). The involvement of WAVE/SCAR and myosins in fertilization have also been shown in both the egg and central cells (5, 7, 9). However, *ROP8* is expressed only in the Arabidopsis central cell (5), and it still remains unknown what counterpart of *ROP8* controls F-actin dynamics for fertilization in the egg cell. This question is also the case with *XI-G*. Interestingly, *SCAR2* appears to be expressed in the Arabidopsis egg cell as the highest among *SCAR* genes as well, with *SCAR3* as the second highest (49). We did not observe sperm nuclear migration delay in *scar2-1* egg cells (*SI Appendix*, Fig. S1). Due to the cell size, the sperm nuclear migration distance within the fertilized egg cell is shorter than that of the fertilized central cell, and indeed, the sperm nuclear migration time is shorter in the egg cell (50). Therefore, it is possible that we simply could not detect sperm nuclear migration phenotypes in the egg cell with our fertilization assay system, and SCAR2 may also play a role in F-actin meshwork movement in the egg cell. Another possibility is that *SCAR3* may control the egg F-actin dynamics for fertilization. The effect of *scar* on sperm nuclear migration in the egg cell should be amplified in the yet-to-be-identified egg *rop* and/or *myosin xi* mutant; thus, investigation of these genes together will facilitate the identification of egg fertilization factors.

In Arabidopsis, rapid sperm chromatin decondensation in the fertilized central cell is required prior to its first mitotic division of the fused triploid nucleus for proper endosperm development (29). One of the reasons why the constant F-actin meshwork movement is already initiated even before pollen tube arrival to the female gametophyte is to ensure the rapid movement of the sperm nucleus immediately after plasmogamy for successful karyogamy and completion of sperm chromatin decondensation prior to the first mitotic division (51). Nevertheless, detailed molecular and cellular mechanisms of flowering plant double fertilization are still lacking. The large central cell enables further understanding of the basis of flowering plant fertilization. Our work uncovers a novel female gametophyte-specific regulatory pathway for F-actin meshwork inward movement and essential roles of *SCAR2* and *XI-G* for sperm nuclear migration in the Arabidopsis central cell. Further investigation will reveal differences and similarities between not only the fertilization processes of the egg and central cells, but also the mechanisms of F-actin dynamics in somatic and reproductive cells.

Materials and Methods

Plant material and growth conditions

All Arabidopsis plant lines used in this work were Columbia-0 (Col-0) ecotype. Seeds were first germinated and seedlings were kept for two weeks under short-day conditions (8 h light, 22°C and 16 h dark, 18°C). Plants were then shifted to 22°C with continuous light. The *proFWA::Lifeact:Venus* (5), *scar2-1* (26), *arp2-1* (20), *dis2-1 (arpc2)* (32), *arpc4-t2* (33) and *proDD65::coxIV:GFP* (38) lines have been described previously. The *proFWA::H2B:mRuby2* and *pro2x35S::lifeact:Venus* constructs were generated in the multisite gateway binary vectors pAlligatorG43 and pAlligatorR43 respectively (5). The *xi-g* (34) (SALK018032C), *scar2-1* (SALK039449) (26) *scar4-1* (SALK_116410C) (13) mutant lines were obtained from the Arabidopsis Biological Resource Center (ABRC). Seeds of *dis2-1 (arpc2)* (32), and *arpc4-t2* (33) mutants were a gift from Dr. Daniel B. Szymanski. The homozygosity of all mutant lines was confirmed by PCR reaction using gene-specific primers flanking the T-DNA insertion site and T-DNA specific primers (*SI Appendix*, Table S1). The *scar2-1, scar4-1, arp2-1, dis2-1, arpc4-t2* and *xi-g* mutant lines were crossed with the *proFWA::Lifeact:Venus* line and homozygous lines were obtained from the F_2 population. The *scar2-1* was crossed with *scar4-1* harbored *proFWA::Lifeact:Venus* marker line to generate double mutants and homozygous line was obtained from the F_2 population.

Fertilization assay

Arabidopsis WT, *xi-g, scar2-1, scar4-1, scar2-1;scar4-1, arp2-1, dis2-1* and *arpc4-t2* pistils were emasculated two days prior to pollination. Pistils were pollinated with the *proHTR10::HTR10:mRFP1* sperm-specific histone marker line (27). Ovules were then dissected 9 hours after pollination and sperm nuclear migration was observed by confocal microscopy.

Plasmid construction and transformation

The promoter sequences of Arabidopsis *XI-G*, *ARP2*, and *DD65* gene were amplified by PCR using the KOD-plus ver. 2 PCR kit (TOYOBO, Japan). Primer sequences for PCR are listed in *SI Appendix*, Table S1 and all constructs were generated by the Multisite Gateway Technology (Invitrogen, CA, USA). The multisite gateway binary vectors pAlligatorR43, pAlligatorG43 and the ENTRY clone plasmids, pENTR221-histone2B and pENTRP2rP3-Clover have been described previously (5). All constructs were transformed into Arabidopsis Col-0 using the floral dip method (52).

F-actin dynamics assay and chemical preparation

Arabidopsis pistils were emasculated two days prior to imaging. Pistils were dissected out by a sharp knife and mature ovules were collected into the assay medium (2.1 g/L Nitsch basal salt mixture, 5% w/v trehalose dehydrate, 0.05% w/v MES KOH (pH 5.8), and 1x Gamborg vitamin) in a glass-bottom dish as described previously (53). For each experiment, ovules from two pistils were collected into 200-µL assay

medium. Myosin inhibitor, BDM (stock, 500 mM in the assay buffer; Sigma-Aldrich, MO, USA) was prepared before each experiment and 20 mM (no incubation) and 50 mM (no incubation) were used as working concentrations. WAVE/SCAR inhibitor, wiskostatin (stock, 10 mM in DMSO; Sigma-Aldrich, MO, USA); ARP2/3 inhibitor CK-666 (stock, 10 mM in DMSO; Sigma-Aldrich, MO, USA); were prepared and kept in -80°C. Freshly prepared working concentration of wiskostatin (10 µM, 1h incubation) and CK-666 (200 µM, 1h incubation) were used.

Imaging

An FV1200 laser scanning confocal system (Olympus) equipped with 488-nm, 515-nm, and 559-nm laser lines and the GaAsP detection filter was used to illuminate Clover, coxIV:GFP, and Alexa Fluor™ 488 (488-nm), Lifeact:Venus (515-nm), and H2B:mRuby2 and HTR10:mRFP1 (559-nm). Snapshot or time-lapse (5 sec to 1 min interval) images with z-planes (15-20 µm total, 3-4 µm each slice) were acquired using FV10-ASW 4.2 software. Laser 3-4%, HV 500-550, gain 1.25 and Kalman 2 options were applied to capture images. All confocal images were analyzed and processed using Fiji (ImageJ) software.

F-actin dynamics quantification

F-actin velocity was measured in two steps. First, kymographs of the F-actin movement were generated with Fiji. Z-projected images of the central cell were processed in Fiji by the following sequence of actions: adjust brightness and contrast; Process > Filters > Gaussian Blur; Process > Background subtraction > Rolling ball radius; adjust brightness and contrast; get kymograph with installed macro in Fiji. Macro was installed from the following link: (http://dev.mri.cnrs.fr/projects/imagej-macros/wiki/Velocity_Measurement_Tool). Second, in the kymograph, segmented lines were drawn to track the movement of actin cables, and velocities were obtained based on the installed macro in Fiji.

F-actin angle and orientation measurement

Z-projected actin cable images, that were processed by setting all pixel values less than 300 to 300 to mask the background noise, were converted to skeletonized images using the LPX imageJ plug-in lineExtract (54) with the default values (*SI Appendix*, Fig. S8*A*). Using a depth-first traversal algorithm, all pixel pairs, of pixels adjacent to each other, in the skeletonized images, were first identified as lines. Then, angles of each pixel pair line relative to the center of the central cell nucleus were determined. Of the pixel pair, whichever pixel was identified second by the depth-first traversal algorithm, was used as the vertex of the angle of the line relative to the center of the nucleus. The angle was calculated using the law of cosines from a triangle generated by the pixel pair and the pixel at the center of the nucleus as vertices. The angle was determined as a 0° to 90° degree angle, subtracting from 180 if necessary. Only lines present between the chalazal end and the top nucleus edge of the central cell were measured due to the quality of the original image.

Mitochondrial Velocity measurement

To calculate mitochondrial velocities, we used the TrackMate plugin (55) in Fiji. All image stacks were cropped to contain only above 52.8 microns on the y-axis. TrackMate ran with an estimated mitochondrial velocity of 1.2 microns, and a threshold of 1. The auto function on initial thresholding removed low-quality mitochondrial predictions. TrackMate ran with the simple LAP tracker to match mitochondrial predictions through time (*SI Appendix*, Fig. S8 *B-D*). The linking maximum distance and gap-closing maximum distance were set to 3 microns. The gap closing maximum frame was set to 2 frames.

Acknowledgments

We are very grateful to Drs. Robert B. Goldberg and Anthony Clark for their critical comments on this manuscript, and Dr. Yukinosuke Ohnishi for image processing. We thank Dr. Daniel B. Szymanski, Purdue University for *dis2-1* and *arpc4-t2* seeds. This work was supported by the National Science Foundation (IOS-1928836 to TK), the National Institute of Food and Agriculture, United States Department of Agriculture (Hatch Program 1014280 to TK), the National Natural Science Foundation of China (31570317 and 31270362 to XP and MS), and the Ministry of Education, Culture, Sports, Science and Technology of Japan Grants-in-Aid for Scientific Research on Innovative Areas (17H05846 and 19H04869 to DM). MFA, UF, and TK were supported by a start-up fund from the Department of Plant and Soil Sciences and the College of Agriculture, Food and Environment, University of Kentucky.

References

1. T. Kawashima, F. Berger, Green love talks; cell–cell communication during double fertilization in flowering plants. *AoB PLANTS* **2011** (2011).

2. J. M. Shin, L. Yuan, M. Ohme-Takagi, T. Kawashima, Cellular dynamics of double fertilization and early embryogenesis in flowering plants. *J. Exp. Zoolog. B Mol. Dev. Evol.* (2020) https:/doi.org/10.1002/jez.b.22981.

3. S. Reinsch, P. Gonczy, Mechanisms of nuclear positioning. *J. Cell Sci.* **111**, 2283–2295 (1998).

4. U. Fatema, M. F. Ali, Z. Hu, A. J. Clark, T. Kawashima, Gamete Nuclear Migration in Animals and Plants. *Front. Plant Sci.* **10** (2019).

5. T. Kawashima, *et al.*, Dynamic F-actin movement is essential for fertilization in Arabidopsis thaliana. *eLife* **3** (2014).

6. Y. Ohnishi, R. Hoshino, T. Okamoto, Dynamics of Male and Female Chromatin during Karyogamy in Rice Zygotes. *Plant Physiol.* **165**, 1533–1543 (2014).

7. X. Peng, T. Yan, M. Sun, The WASP-Arp2/3 complex signal cascade is involved in actin-dependent sperm nuclei migration during double fertilization in tobacco and maize. *Sci. Rep.* **7**, 43161 (2017).

8. T. Kawashima, F. Berger, The central cell nuclear position at the micropylar end is maintained by the balance of F-actin dynamics, but dispensable for karyogamy in Arabidopsis. *Plant Reprod.* **28**, 103–110 (2015).

9. Y. Ohnishi, T. Okamoto, Nuclear migration during karyogamy in rice zygotes is mediated by continuous convergence of actin meshwork toward the egg nucleus. *J. Plant Res.* **130**, 339–348 (2017).

10. H. Lodish, *et al.*, The Dynamics of Actin Assembly. *Mol. Cell Biol. 4th Ed.* (Freeman & Co., 2000).

11. C. Craddock, I. Lavagi, Z. Yang, New Insights into Rho signaling from plant ROP/Rac GTPases. *Trends Cell Biol.* **22**, 492–501 (2012).

12. Z. Yang, Y. Fu, ROP/RAC GTPase signaling. *Curr. Opin. Plant Biol.* **10**, 490–494 (2007).

13. J. F. Uhrig, *et al.*, The role of Arabidopsis SCAR genes in ARP2-ARP3-dependent cell morphogenesis. *Dev. Camb. Engl.* **134**, 967–977 (2007).

14. M. Yanagisawa, C. Zhang, D. B. Szymanski, ARP2/3-dependent growth in the plant kingdom: SCARs for life. *Front. Plant Sci.* **4** (2013).

15. D. Basu, *et al.*, DISTORTED3/SCAR2 is a putative arabidopsis WAVE complex subunit that activates the Arp2/3 complex and is required for epidermal morphogenesis. *Plant Cell* **17**, 502–524 (2005).

16. M. Frank, *et al.*, Activation of Arp2/3 complex-dependent actin polymerization by plant proteins distantly related to Scar/WAVE. *Proc. Natl. Acad. Sci.* **101**, 16379–16384 (2004).

17. J. D. Rotty, C. Wu, J. E. Bear, New insights into the regulation and cellular functions of the ARP2/3 complex. *Nat. Rev. Mol. Cell Biol.* **14**, 7–12 (2013).

18. R. Dyche Mullins, T. D. Pollard, Structure and function of the Arp2/3 complex. *Curr. Opin. Struct. Biol.* **9**, 244–249 (1999).

19. C. Zhang, *et al.*, Arabidopsis SCARs Function Interchangeably to Meet Actin-Related Protein 2/3 Activation Thresholds during Morphogenesis. *Plant Cell* **20**, 995–1011 (2008).

20. S. Li, L. Blanchoin, Z. Yang, E. M. Lord, The Putative Arabidopsis Arp2/3 Complex Controls Leaf Cell Morphogenesis. *Plant Physiol.* **132**, 2034 (2003).

21. J. Le, S. E.-D. El-Assal, D. Basu, M. E. Saad, D. B. Szymanski, Requirements for Arabidopsis ATARP2 and ATARP3 during Epidermal Development. *Curr. Biol.* **13**, 1341–1347 (2003).

22. J. R. Peterson, *et al.*, Chemical inhibition of N-WASP by stabilization of a native autoinhibited conformation. *Nat. Struct. Mol. Biol.* **11**, 747 (2004).

23. R. Rohatgi, *et al.*, The Interaction between N-WASP and the Arp2/3 Complex Links Cdc42-Dependent Signals to Actin Assembly. *Cell* **97**, 221–231 (1999).

24. M. W. Schmid, *et al.*, A powerful method for transcriptional profiling of specific cell types in eukaryotes: laser-assisted microdissection and RNA sequencing. *PloS One* **7**, e29685 (2012).

25. A. Schmidt, M. W. Schmid, U. Grossniklaus, Analysis of plant germline development by high-throughput RNA profiling: technical advances and new insights. *Plant J.* **70**, 18–29 (2012).

26. X. Zhang, J. Dyachok, S. Krishnakumar, L. G. Smith, D. G. Oppenheimer, IRREGULAR TRICHOME BRANCH1 in Arabidopsis Encodes a Plant Homolog of the Actin-Related Protein2/3 Complex Activator Scar/WAVE That Regulates Actin and Microtubule Organization. *Plant Cell* **17**, 2314–2326 (2005).

27. M. Ingouff, Y. Hamamura, M. Gourgues, T. Higashiyama, F. Berger, Distinct Dynamics of HISTONE3 Variants between the Two Fertilization Products in Plants. *Curr. Biol.* **17**, 1032–1037 (2007).

28. S. J. Aw, Y. Hamamura, Z. Chen, A. Schnittger, F. Berger, Sperm entry is sufficient to trigger division of the central cell but the paternal genome is required for endosperm development in Arabidopsis. *Dev. Camb. Engl.* **137**, 2683–2690 (2010).

29. D. Maruyama, T. Higashiyama, T. Endo, S.-I. Nishikawa, Fertilization-Coupled Sperm Nuclear Fusion is Required for Normal Endosperm Nuclear Proliferation. *Plant Cell Physiol.* (2019) https:/doi.org/10.1093/pcp/pcz158.

30. B. J. Nolen, *et al.*, Characterization of two classes of small molecule inhibitors of Arp2/3 complex. *Nature* **460**, 1031–1034 (2009).

31. B. Hetrick, M. S. Han, L. A. Helgeson, B. J. Nolen, Small molecules CK-666 and CK-869 inhibit Arp2/3 complex by blocking an activating conformational change. *Chem. Biol.* **20**, 701–712 (2013).

32. S. El-Din El-Assal, J. Le, D. Basu, E. L. Mallery, D. B. Szymanski, DISTORTED2 encodes an ARPC2 subunit of the putative Arabidopsis ARP2/3 complex. *Plant J. Cell Mol. Biol.* **38**, 526–538 (2004).

33. S. O. Kotchoni, *et al.*, The association of the Arabidopsis actin-related protein2/3 complex with cell membranes is linked to its assembly status but not its activation. *Plant Physiol.* **151**, 2095–2109 (2009).

34. V. V. Peremyslov, A. I. Prokhnevsky, D. Avisar, V. V. Dolja, Two Class XI Myosins Function in Organelle Trafficking and Root Hair Development in Arabidopsis. *Plant Physiol.* **146**, 1109–1116 (2008).

35. C. J. Staiger, *et al.*, Actin filament dynamics are dominated by rapid growth and severing activity in the Arabidopsis cortical array. *J. Cell Biol.* **184**, 269–280 (2009).

36. C. Cai, J. L. Henty-Ridilla, D. B. Szymanski, C. J. Staiger, Arabidopsis Myosin XI: A Motor Rules the Tracks. *Plant Physiol.* **166**, 1359–1370 (2014).

37. J. Šamaj, M. Peters, D. Volkmann, F. Baluška, Effects of Myosin ATPase Inhibitor 2,3-Butanedione 2-Monoxime on Distributions of Myosins, F-Actin, Microtubules, and Cortical Endoplasmic Reticulum in Maize Root Apices. *Plant Cell Physiol.* **41**, 571–582 (2000).

38. D. Maruyama, *et al.*, Rapid Elimination of the Persistent Synergid through a Cell Fusion Mechanism. *Cell* **161**, 907–918 (2015).

39. H. Ueda, *et al.*, Myosin-dependent endoplasmic reticulum motility and F-actin organization in plant cells. *Proc. Natl. Acad. Sci. U. S. A.* **107**, 6894–6899 (2010).

40. D. Basu, S. E.-D. El-Assal, J. Le, E. L. Mallery, D. B. Szymanski, Interchangeable functions of Arabidopsis PIROGI and the human WAVE complex subunit SRA1 during leaf epidermal development. *Dev. Camb. Engl.* **131**, 4345–4355 (2004).

41. D. Basu, J. Le, T. Zakharova, E. L. Mallery, D. B. Szymanski, A SPIKE1 signaling complex controls actin-dependent cell morphogenesis through the heteromeric WAVE and ARP2/3 complexes. *Proc. Natl. Acad. Sci. U. S. A.* **105**, 4044–4049 (2008).

42. S. E.-D. El-Assal, J. Le, D. Basu, E. L. Mallery, D. B. Szymanski, Arabidopsis GNARLED encodes a NAP125 homolog that positively regulates ARP2/3. *Curr. Biol. CB* **14**, 1405–1409 (2004).

43. D. Susaki, *et al.*, Dynamics of the cell fate specifications during female gametophyte development in Arabidopsis. *bioRxiv*, 2020.04.07.023028 (2020).

44. D. Mizuno, C. Tardin, C. F. Schmidt, F. C. MacKintosh, Nonequilibrium Mechanics of Active Cytoskeletal Networks. *Science* **315**, 370–373 (2007).

45. G. H. Koenderink, *et al.*, An active biopolymer network controlled by molecular motors. *Proc. Natl. Acad. Sci.* **106**, 15192–15197 (2009).

46. D. Pruyne, *et al.*, Role of Formins in Actin Assembly: Nucleation and Barbed-End Association. *Science* **297**, 612–615 (2002).

47. S. L. Madison, A. Nebenführ, Understanding myosin functions in plants: are we there yet? *Curr. Opin. Plant Biol.* **16**, 710–717 (2013).

48. K. Tamura, *et al.*, Myosin XI-i Links the Nuclear Membrane to the Cytoskeleton to Control Nuclear Movement and Shape in Arabidopsis. *Curr. Biol.* **23**, 1776–1781 (2013).

49. P. Zhao, *et al.*, Two-Step Maternal-to-Zygotic Transition with Two-Phase Parental Genome Contributions. *Dev. Cell* **49**, 882-893.e5 (2019).

50. Y. Hamamura, *et al.*, Live-Cell Imaging Reveals the Dynamics of Two Sperm Cells during Double Fertilization in Arabidopsis thaliana. *Curr. Biol.* **21**, 497–502 (2011).

51. T. Kawashima, Male chromatin needs to relax to get seeds started. *Plant Cell Physiol.* https:/doi.org/10.1093/pcp/pcz211 (November 17, 2019).

52. S. J. Clough, A. F. Bent, Floral dip: a simplified method for Agrobacterium-mediated transformation of Arabidopsis thaliana. *Plant J. Cell Mol. Biol.* **16**, 735–743 (1998).

53. K. Gooh, *et al.*, Live-Cell Imaging and Optical Manipulation of Arabidopsis Early Embryogenesis. *Dev. Cell* **34**, 242–251 (2015).

54. T. Higaki, Quantitative evaluation of cytoskeletal organizations by microscopic image analysis. *PLANT Morphol.* **29**, 15–21 (2017).

55. J.-Y. Tinevez, *et al.*, TrackMate: An open and extensible platform for single-particle tracking. *Methods San Diego Calif* **115**, 80–90 (2017).

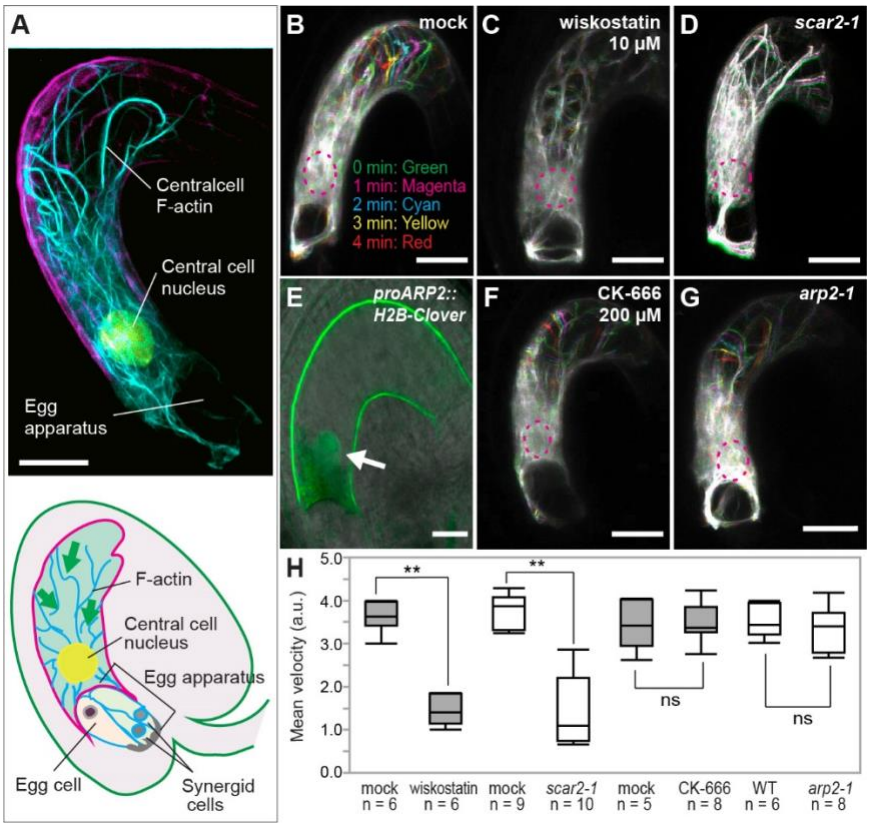

Fig. 1. F-actin dynamics in the central cell is WAVE/SCAR dependent, but ARP2/3 complex independent. (*A*) (Top) Z-projected confocal image of the central cell F-actin (cyan, *proFWA::lifeact:Venus*), central cell nucleus (yellow, *proFWA::H2B:mRuby2*), and autofluorescence (magenta) marking the central cell border. (Bottom) Schematic diagram of the mature Arabidopsis ovule. Arrows indicate the direction of central cell F-actin movement from the plasma membrane periphery to the nucleus. (*B-D;F-G*) Time-lapse (one-minute interval, marked by five different colors) stacks of Z-projected central cell F-actin images of the mock treatment (*B*), wiskostatin (10 µM for 1h incubation) treatment (*C*), *scar2-1* mutant (*D*), CK-666 (200 µM for 1h incubation) treatment (*F*), and the *arp2-1* mutant (*G*). Dashed circles indicate the position of the central cell nucleus. F-actin marked by different colors denotes F-actin movement, whereas white color resulting from overlapping of all colors represents less or no movement. (*E*) The transcriptional activity of the Arabidopsis *ARP2* promoter is visualized by *proARP2::H2B:Clover* (green). Arrow points to the central cell nucleus and autofluorescence marks the central cell border. (*H*) Mean velocity of F-actin dynamics in the central cell (**, $p < 0.001$; ns, not significant; Tukey-Kramer HSD test). The box spans first and third quartiles, and the line inside the box shows the median. Bars on the top and bottom represent the maximum and minimum values. Scale bar = 20 µm.

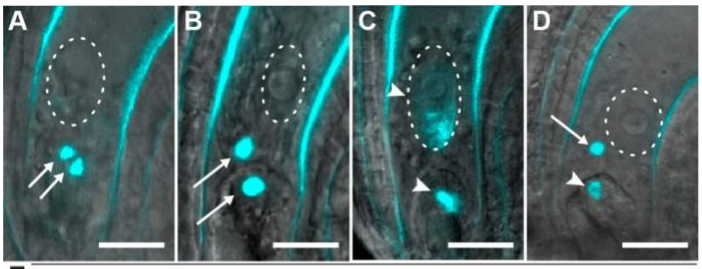

E

Group	Gene	Stage A	Stage B	Stage C	Stage D	% of stage D
	WT	13	32	139	0	**0**
SCARs	*scar2-1*	2	7	77	44	**33.9**
	scar4-1	11	7	71	0	**0**
	scar2-1;scar4-1	5	7	67	44	**35.8**
ARP2/3	*arp2-1*	8	7	78	0	**0**
	dis2-1	4	6	116	0	**0**
	arpc4-t2	3	29	116	0	**0**
Myosin XI	*xi-g*	9	19	92	80	**40**

Fig. 2. Sperm nuclear migration is delayed in *scar2-1* and *xi-g* central cells. (*A-D*) Representative images of sperm chromatin dynamics: sperm cells just released from the pollen tube into the ovule (*A*); sperm nuclei started moving towards the central cell and egg cell nuclei (*B*); sperm chromatin became decondensed in both the central cell and egg cell nuclei (*C*); and delayed karyogamy and sperm chromatin decondensation observed in the *scar2-1* central cell (*D*). Note that sperm chromatin became fully decondensed in the egg cell nucleus while sperm chromatin remained condensed in the central cell. This delayed phenotype was not observed in WT. Sperm chromatin was visualized by the sperm-specific histone marker *proHTR10::HTR10:mRFP1*. Arrows and arrowheads point to the condensed and decondensed sperm chromatin, respectively. Dashed circles indicate the position of the central cell nucleus. Autofluorescence of the central cell border was also visualized. (*E*) Status of sperm chromatin 9 hours after pollination. Stage A-D are shown in panel A-D, respectively. Scale bar = 20 μm.

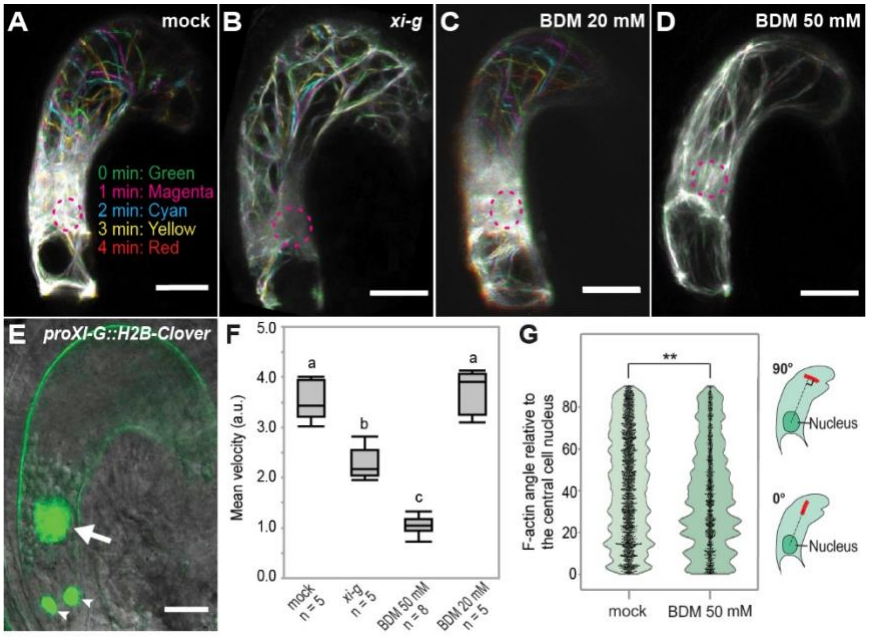

Fig. 3. The class XI myosin, XI-G, is involved in F-actin meshwork movement in the Arabidopsis central cell. (*A*-*D*) Time-lapse (one-minute interval, marked by five different colors) stacks of Z-projected central cell F-actin images of the mock treatment (*A*), the *xi-g* mutant (*B*), 20 mM BDM treatment (*C*), and 50 mM BDM treatment (*D*). Dashed circles indicate the position of the central cell nucleus. F-actin marked by different colors denotes F-actin movement, whereas white color resulting from overlapping of all colors, represents less or no movement. (*E*) The transcriptional activity of the Arabidopsis *XI-G* promoter is visualized by *proXI-G::H2B:Clover* (green). Autofluorescence marks the central cell wall; the arrow and arrowheads point to the central cell nucleus and synergid nuclei respectively. (*F*) Mean velocity of F-actin dynamics in the central cell. Levels not connected by the same letter (a,b,c) are significantly different ($p < 0.01$, Tukey-Kramer HSD test). The box spans first and third quartiles, and the line inside the box shows the median. Bars on the top and bottom represent the maximum and minimum values. (*G*) The orientation of F-actin in the central cell was evaluated by measuring the angles of F-actin cables (shown in red) made with a line radiating from the center of the central cell nucleus (shown as dashed lines). Black dots represent individual angle data and violin shapes show the kernel probability densities (**, $p < 0.001$; Tukey-Kramer HSD test). Scale bar = 20 µm.

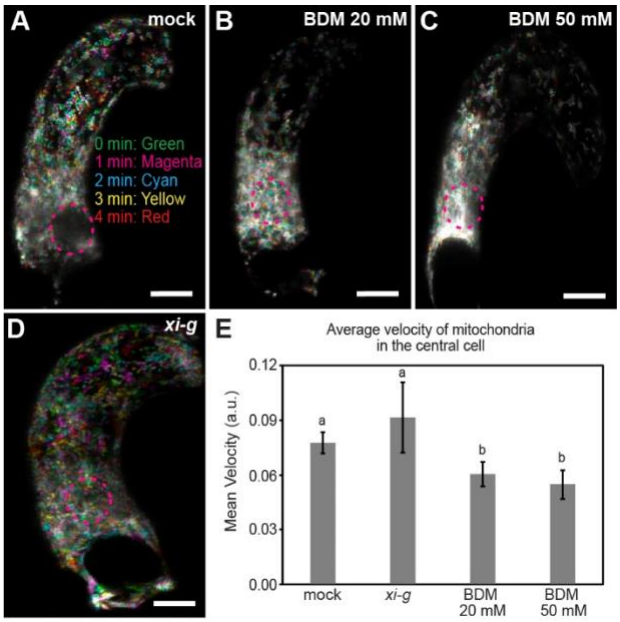

Fig. 4. 20 mM BDM affects mitochondrial movement in the Arabidopsis central cell. (*A*-*D*) Time-lapse (one-min interval, marked by five different colors) stacks of Z-projected central cell mitochondrial movement images of the mock treatment (*A*), 20 mM BDM treatment (*B*), 50 mM BDM treatment (*C*) and in *xi-g* mutant (*D*). Mitochondria marked by different colors denote movement, whereas white color resulting from overlapping of all colors represents less or no movement. Dashed circles indicate the position of the central cell nucleus. (*E*) Average velocity of mitochondrial movement in the central cell. Error bars represent SEM. Levels not connected by the same letter (a and b) are significantly different ($p < 0.01$, Tukey-Kramer HSD test). Scale bar = 20 µm.

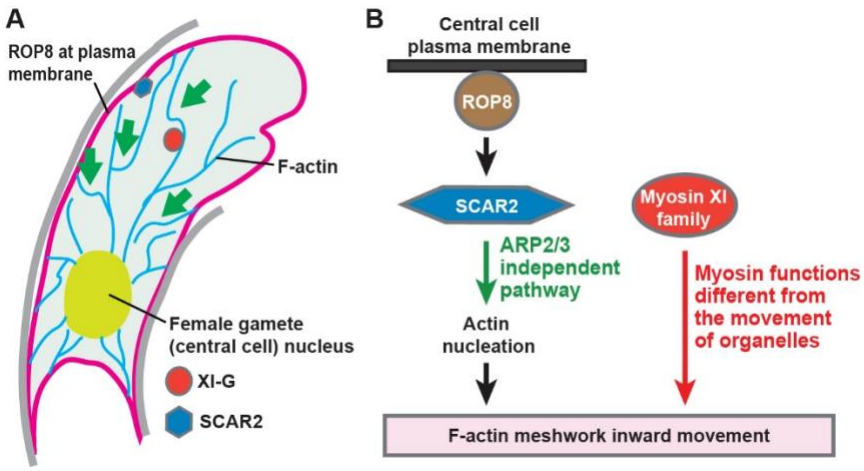

Fig. 5. Model of F-actin dynamics in the female gamete for sperm nuclear migration. (*A*-*B*) Schematic image of F-actin meshwork movement (*A*) and the pathway controlling F-actin movement in the Arabidopsis central cell (*B*). ROP8 localizes to the plasma membrane and interacts with SCAR2. The ROP8-SCAR2 signaling pathway positively regulates the meshwork F-actin movement in a novel gametophyte-specific ARP2/3 independent manner. Myosins including XI-G also regulate the meshwork F-actin movement through myosin functions distinguishable from the movement of organelles.

PNAS
www.pnas.org

Supplementary Information for

ARP2/3-Independent WAVE/SCAR Pathway and Class XI Myosin Control Sperm Nuclear Migration in Flowering Plants

Mohammad Foteh Ali[a], Umma Fatema[a], Xiongbo Peng[b], Samuel W. Hacker[c], Daisuke Maruyama[d], Mengxiang Sun[b], Tomokazu Kawashima[a,c,1]

[a]Department of Plant and Soil Sciences, University of Kentucky, Lexington, KY, 40546-0312

[b]State Key Laboratory of Hybrid Rice, College of Life Science, Wuhan University, Wuhan, 430072, China

[c]Agriculture and Medical Biotechnology Program, University of Kentucky, Lexington, KY, 40546-0312

[d]Kihara Institute for Biological Research, Yokohama City University, Yokohama, Kanagawa 244-0813, Japan

[1]To whom correspondence may be addressed. Email: tomo.k@uky.edu

This PDF file includes:

Other supplementary materials for this manuscript include the following:

Movies S1 to S4

Supplementary Materials and Methods

Tobacco *in vitro* assay

Tobacco central cell isolation from ovules, sperm cell isolation from flowers, and *in vitro* fusion of the tobacco sperm cell with the central cell were performed according to previously published methods (1, 2). For *in vitro* fusion, polyethylene glycol (PEG) medium was prepared that contained 5 mM $CaCl_2$, 3 mM 2-(*N*-morpholino)ethanesulfonic acid (MES), 20% (W/V) PEG and 5% (W/V) mannitol and pH was adjusted to 6.0.

CK-666 effect on Arabidopsis cotyledon pavement cell

8-day-old Arabidopsis (Col-0) seedlings grown on a 1/2 Murashige and Skoog (MS) medium (Phyto Technology Laboratories) plate were submerged in the assay medium (2.1 g/L Nitsch basal salt mixture, 5% w/v trehalose dehydrate, 0.05% w/v MES-KOH (pH 5.8), and 1x Gamborg vitamin) (3) with DMSO (Mock) or 200 μM of CK-666 for one hour at room temperature. The dissected cotyledon was then mounted on a glass slide for confocal microscopy.

Arabidopsis cotyledon pavement cell F-actin angle analysis

The orientations (-90° to 90°) of F-actin relative to the long axes of cotyledon pavement cells were analyzed with Fiji (4). First, max intensity z-projected F-actin images *(pro2x35s::Lifeact:Venus* in Col-0) of individual cotyledon pavement cells were cropped. For each cell, the long axis was drawn manually (*SI Appendix*, Fig. S3*A*). The F-actin angles relative to the image x-axes were first obtained in Fiji by the following sequence of actions: Analyze > Directionality > Local gradient orientation with NBins set to 181. The angles were then adjusted to relative to the long axes of cotyledon pavement cells in Fiji. For each treatment, 18-20 individual cotyledon pavement cells were analyzed and averaged.

Phalloidin F-actin immunostaining

Phalloidin F-actin immunostaining was performed as described (5). In brief, 10-day-old Arabidopsis (Col-0) seedlings were fixed with 4% fresh formaldehyde in PME buffer (50 mM PIPES, 5 mM $MgSO_4$, 5 mM EGTA, pH 6.8) for 30 minutes with vacuum, followed by 1.5 h without vacuum on ice. The seedlings were then rinsed three times with PME buffer and the dissected cotyledons were incubated in 0.33 μM phalloidin (Invitrogen™, Alexa Fluor™ 488 Phalloidin) in PME buffer with 0.03% Triton X-100 for one hour at room temperature in dark conditions. The samples were rinsed three times by PME buffer and mounted on a glass slide for confocal microscopy.

Agrobacterium-mediated Arabidopsis transformation for transient expression (agroinfiltration)

The *Agrobacterium*-mediated Arabidopsis transformation for Lifeact:Venus transient expression was performed as described (6). The *Agrobacterium* harboring *pro2x35S::Lifeact:Venus* was grown on a YEB medium plate (1 g/L yeast extract, 5 g/L beef extract, 5 g/L peptone, 5 g/L sucrose, 0.5 g/L $MgSO_4$ $7H_2O$,

1 g/L NH_4Cl, 0.15 g/L KCl, 0.01 g/L $CaCl_2$, 0.0025 g/L $FeSO_4$ $7H_2O$, 2 mM Phosphate buffer [pH 5.5], 1% glucose, 20 mM MES [pH 5.5], 200 µM acetosyringone, 1 % agar) with appropriate antibiotics at 28°C for 48 hours. The *Agrobacterium* cells were scraped from the plate, resuspend in 500 µl of the washing solution (10 mM $MgCl_2$, 100 µM acetosyringone), and further diluted in the infiltration solution (1/4 MS [pH 6.0], 1% sucrose, 100 µM acetosyringone, 0.005% [v/v] Silwet L-77) to an OD_{600} of 0.5. The *Agrobacterium* cells were infiltrated with a 1 mL plastic syringe into the abaxial side of 4-week-old Arabidopsis rosette leaves (WT and *arp2-1*). The plants were kept under light for 1 h, followed by dark for 1 day and light for 2 days at room temperature. Squares of tissue were cut from around infiltrated area of the transformed leaves and mounted on glass slides with 10% glycerol for confocal microscopy.

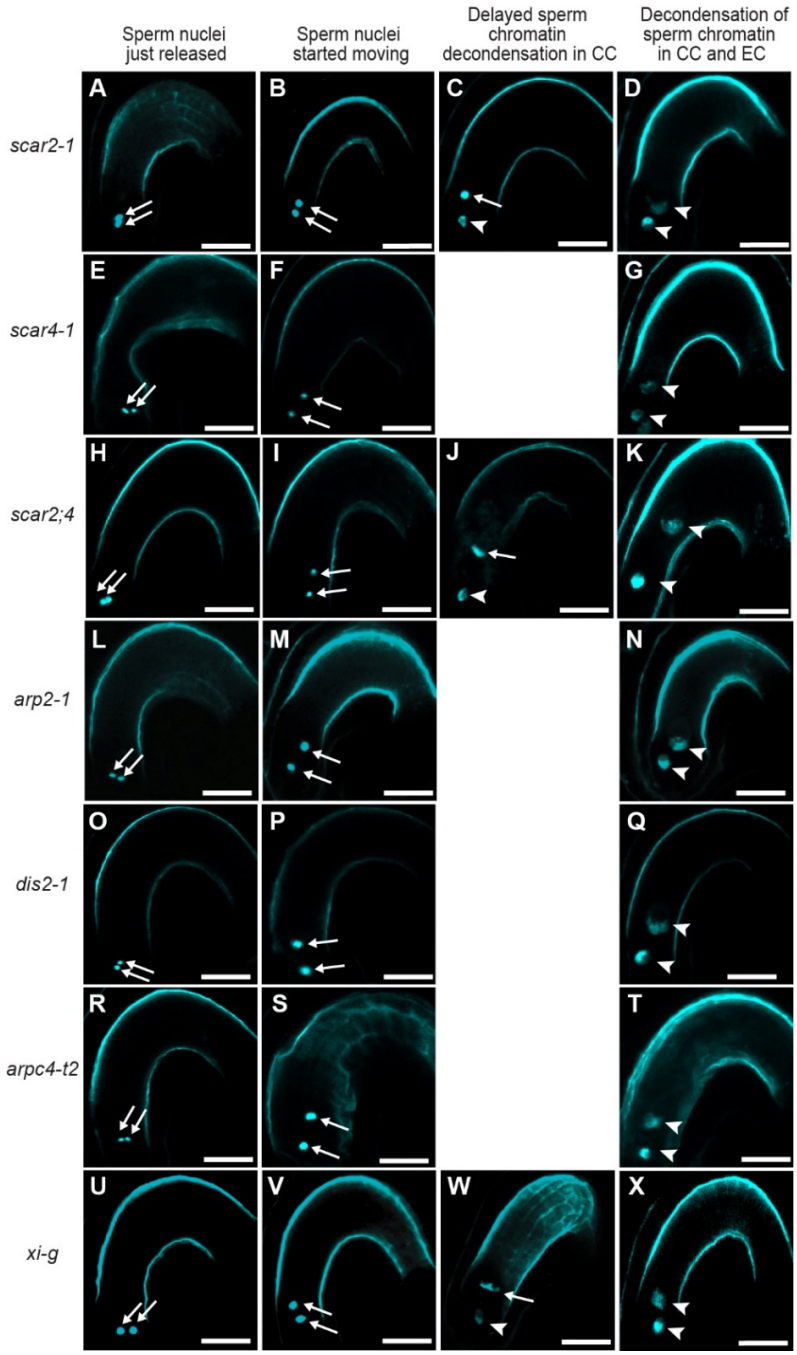

Fig. S1. Sperm nuclear migration is delayed in the *scar2-1, scar2-1;scar4-1* and *xi-g.* (*A-X*) Representative images of sperm nuclear movement in the central cell of *scar2-1* (*A-D*), *scar4-1* (*E-G*), *scar2;4* double mutant (*H-K*), *arp2-1* (*L-N*), *dis2-1* (*O-Q*), *arpc4-t2* (*R-T*) and *xi-g* (*U-X*). Sperm cells just released in the ovule (1st column), sperm nuclei started moving towards the central cell nucleus and egg cell nucleus (2nd column), delayed or no sperm chromatin decondensation occurred in central cell while sperm chromatin already became decondensed in the egg cell nucleus (3rd column) which was not observed in *scar4-1*, *arp2-1, dis2-1, and arpc4-t2* and sperm chromatin became decondensed in both the central cell nucleus and egg cell nucleus (4th column), Sperm chromatin was visualized by the sperm-specific histone marker *proHTR10::HTR10:mRFP1*. Arrows and arrowhead point to the condensed and decondensed sperm chromatin, respectively. Autofluorescence of the central cell border was also visualized. Scale bar = 20 μm.

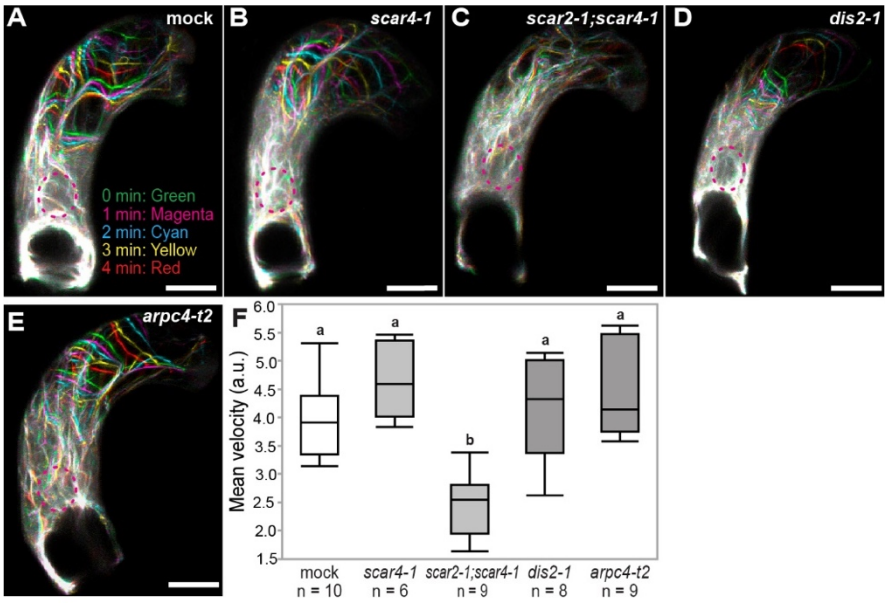

Fig. S2. F-actin dynamics in the central cell is WAVE/SCAR dependent, but ARP2/3 complex independent. (*A*-*E*) Time-lapse (one-minute interval, marked by five different colors) stacks of Z-projected central cell F-actin images of the mock treatment (*A*), *scar4-1* mutant (*B*), *scar2-1;scar4-1* double mutants (*C*), *dis2-1* mutant (*D*) and *arpc4-t2* mutant (*E*). Dashed circles indicate the position of the central cell nucleus. F-actin marked by different colors denotes F-actin movement, whereas white color resulting from overlapping of all colors represents less or no movement. (*F*) Mean velocity of F-actin dynamics in the central cell. The box spans first and third quartiles, and the line inside the box shows the median. Bars on the top and bottom represent the maximum and minimum values. Levels not connected by the same letter (a and b) are significantly different ($p < 0.001$, Tukey-Kramer HSD test). Scale bar = 20 μm.

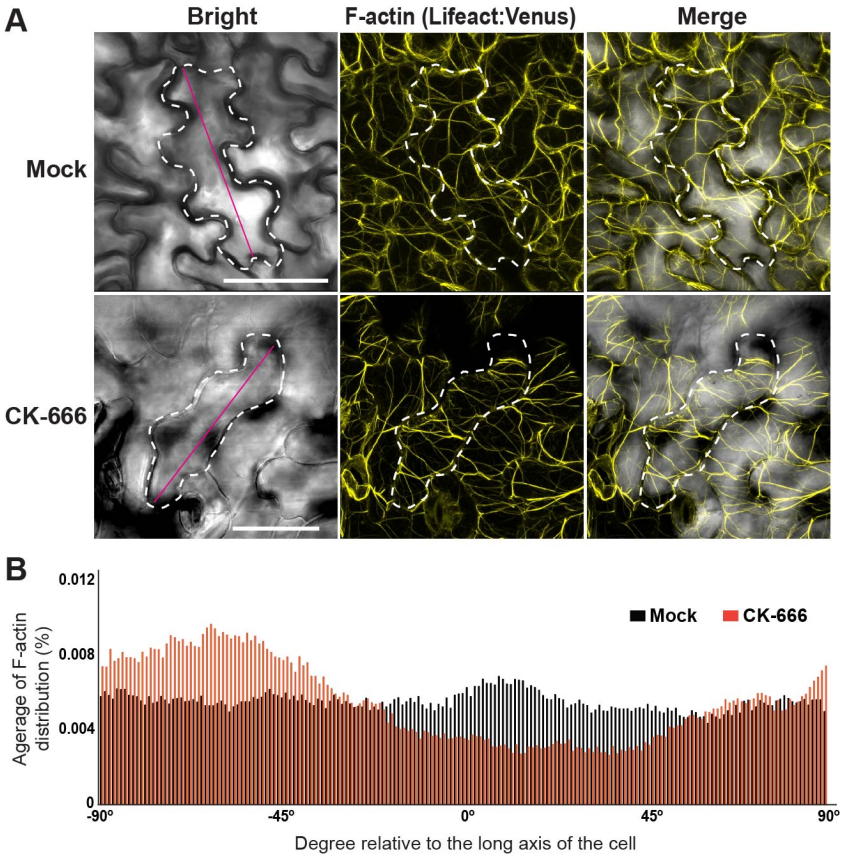

Fig. S3. CK-666 treatment alters the F-actin orientation. (*A*) Z-projected images of F-actin (*pro2x35S::Lifeact:Venus* in Col-0) in the abaxial side of cotyledon pavement cells treated without (Mock) and with CK-666 (200 μM, 1 hour incubation). CK-666 treatment re-oriented F-actin perpendicular to the long axis of the pavement cell. The dashed-white and magenta lines indicate a pavement cell shape and the long axis of the cell, respectively. (*B*) The average distribution of F-actin degree of orientation relative to the long axis of the pavement cell (n = 20 and 18 cells for Mock and CK-666 treatment, respectively). Scale bar = 50 μm.

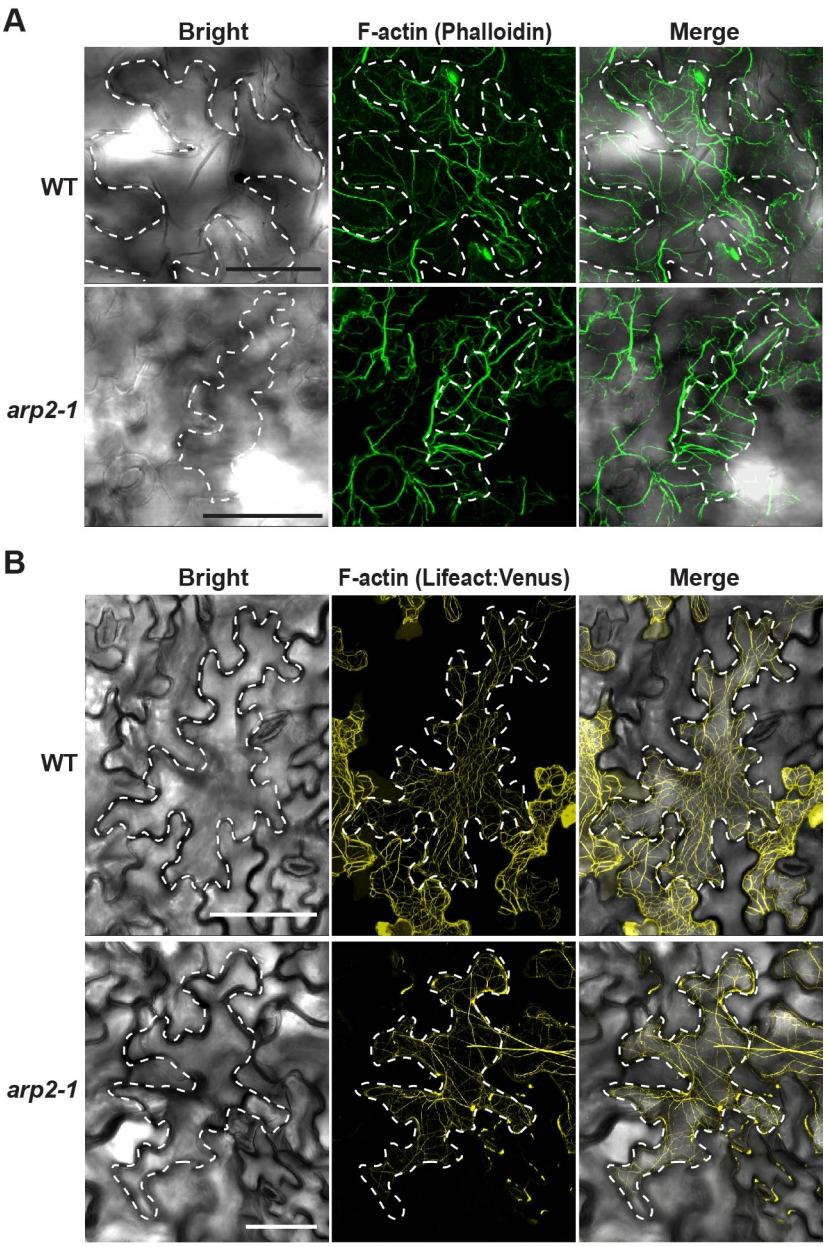

Fig. S4. F-actin organization in WT and *arp2-1.* (*A*) Z-projected images of F-actin (phalloidin immunostaining) in the abaxial side of WT and *arp2-1* cotyledon pavement cells. (*B*) Z-projected images of F-actin (*pro2x35S::Lifeact:Venus* agroinfiltration) in the abaxial side of WT and *arp2-1* rosette leaf pavement cells. As previously described (7), the F-actin orientation in *arp2-1* is more perpendicular to the long axis of the cell compared to WT (Col-0). The dashed-white line indicates a cell shape. Scale bar = 50 μm.

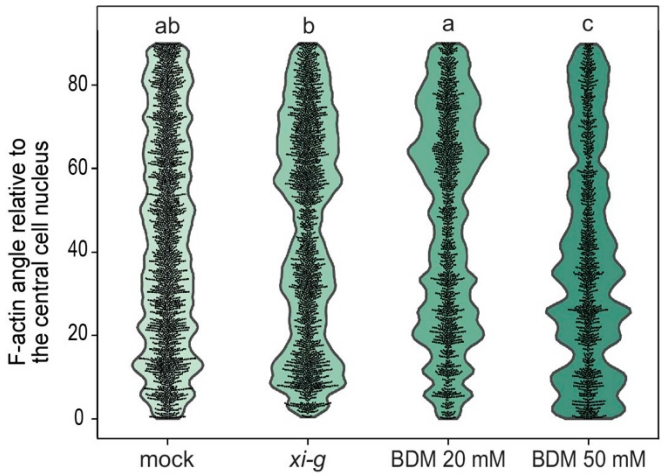

Fig. S5. 50 mM BDM affects the orientation of F-actin in the central cell. The orientation of F-actin in the central cell was evaluated by measuring the angles of F-actin cables made with a line radiating from the center of the central cell nucleus. Black dots represent individual angle data and violin shapes show the kernel probability densities. Levels not connected by the same letter (a,b,c) are significantly different (p < 0.001, Tukey-Kramer HSD test).

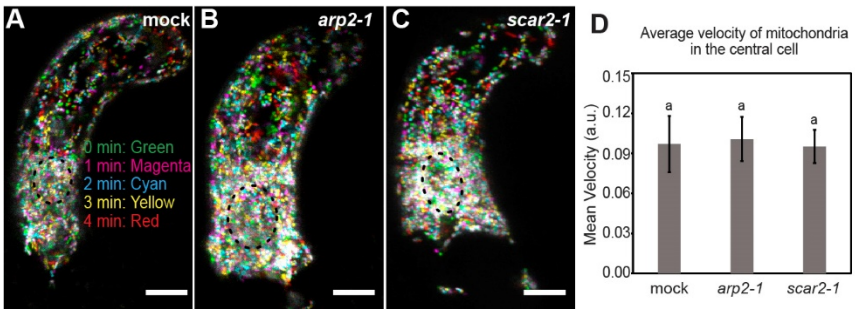

Fig. S6. ARP2 and SCAR2 independent mitochondrial movement in the Arabidopsis central cell. (*A*-*C*) Time-lapse (one-min interval, marked by five different colors) stacks of Z-projected central cell mitochondrial movement images of the mock treatment (*A*), *arp2-1* (*B*) and *scar2-1* (C) mutants. Mitochondria marked by different colors denote movement, whereas white color resulting from overlapping of all colors represents less or no movement. Dashed circles indicate the position of the central cell nucleus. (*D*) Average velocity of mitochondrial movement in the central cell. Error bars represent SEM. Levels connected by the same letter (a) are not significantly different ($p < 0.01$, Tukey-Kramer HSD test). Scale bar = 20 μm.

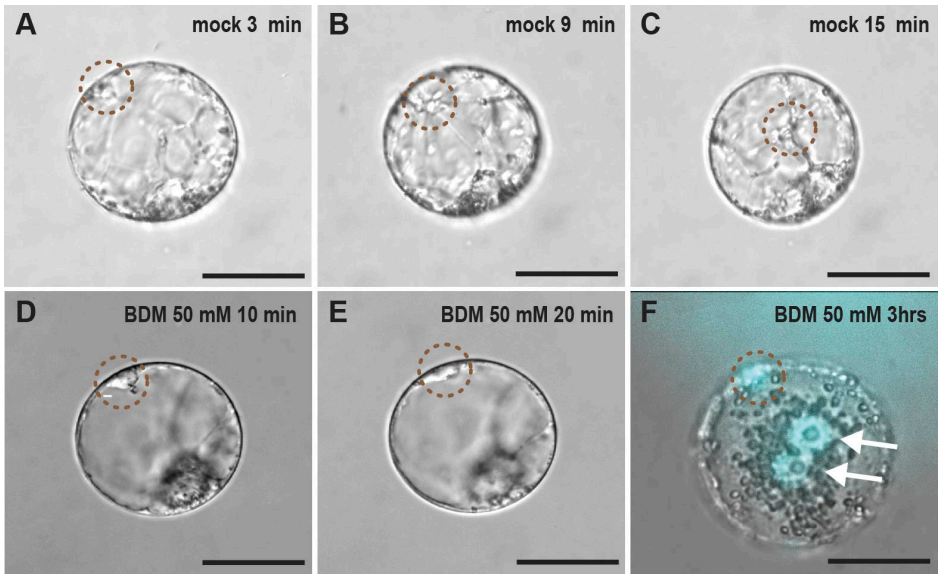

Fig. S7. Myosin function is also required for sperm nuclear migration in the tobacco central cell. (*A*-*F*) Time-lapse images showing *in vitro* fusion of the tobacco sperm nucleus with the central cell nucleus. In mock, sperm nucleus is moving toward the central cell polar nuclei (*A*-*C*). 15 min after nuclear fusion, the sperm nucleus already migrated towards the central cell polar nuclei (*C*). Sperm nuclear migration stopped with 50 mM BDM treatment (*D* and *E*), and the sperm nucleus remained at the entry position even after three hours incubation (*F*). Merged image of bright field and DAPI fluorescence (cyan) shows the static position of the sperm nucleus (*F*). Dashed circles indicate the position of the incorporated sperm nucleus. Arrows point to the central cell polar nuclei. Scale bar = 50 μm.

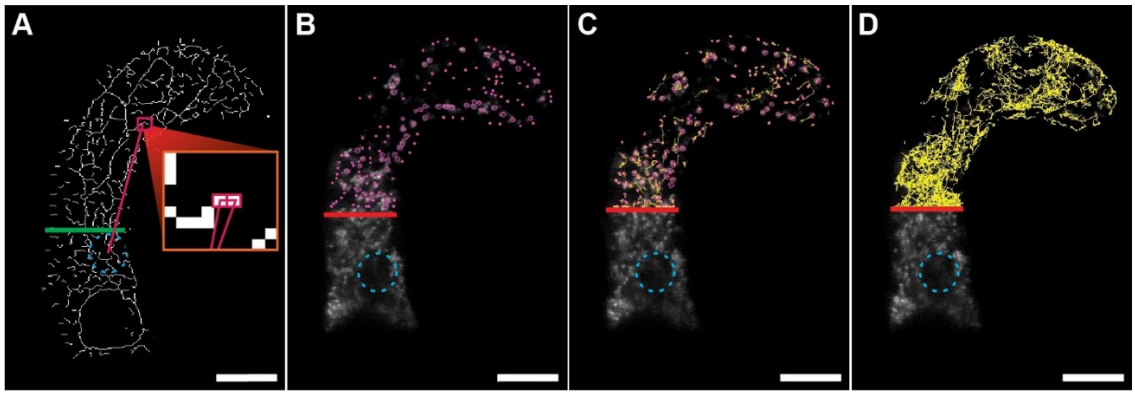

Fig. S8. Scheme of F-actin orientation and mitochondrial velocity measurement in the central cell. (*A*) Stack of Z-projected skeletonized image shows the orientation of actin cables. The orientation of F-actin in the central cell was estimated by measuring the angles actin cables made with a line (example shown in magenta) radiating from the center of the central cell nucleus. The rectangular insert represents a zoomed region of F-actin containing a pixel pair line that was used for angle measurement. Angles were measured only above the green line present at the top nucleus edge of the central cell. (*B*-*D*) The time-lapse stack image shows mitochondria in the central cell. Open and filled circles show mitochondria in the present and previous frames, respectively (*B*). Yellow lines represent the movement of mitochondria between two frames (*C*) and all frames (*D*). Mitochondria only above the red line were selected for velocity measurement. Dashed circles indicate the position of the central cell nucleus. Scale bar = 20 μm.

Table S1. The list of oligonucleotide sequences used in this study.

Amplified fragment	Purpose	Position	Sequence (5'-3')
A part of the *XI-G* gene	*xi-g* genotyping	Fw	tgtgtgcagtccaatcctg
		Rv	tgggcttagaaaacactgcca
proXI-G	Cloning the *XI-G* promoter into pDONR-P4P1r	Fw	attB4-atgagcatatgaaagagtgtctca
		Rv	attB1r-gttcaatctctgtatcaacgacaga
A part of the *ARP2* gene	*arp2-1* genotyping	Fw	ccattcctatctgggtttcg
		Rv	ttctcctgcttcttcttgcc
proARP2	Cloning the *ARP2* promoter into pDONR-P4P1r	Fw	attB4-ctgagtgagagtgataatctatacttattgaaa
		Rv	attB1r-cttctccgatttctatagagactacagatt
A part of the *ARPC4* gene	*arpc4-t2* genotyping	Fw	cctgcaatttccatggttaaa
		Rv	tggtaaatgcatcacgaattg
A part of the *ARPC2* gene	*dis2-1* genotyping	Fw	ctgtgtatcacaggcggataa
		Rv	taattgctacaagcctatccag
A part of the *SCAR2* gene	*scar2-1* genotyping	Fw	tatggctggtctcgttggcat
		Rv	tgctcatggtgttttgaatgtg
A part of the *SCAR4* gene	*scar4-1* genotyping	Fw	cgaagcagacttcccttcag
		Rv	acccaaatgtgcatttttca
pro2×35S	Cloning the 2×35S promoter into pDONR-P4P1r	Fw	attB4-ggcgtgcctgcaggtcaa
		Rv	attB1r-gggatcctctagagtcgaggt
	attB sequences for Gateway cloning	attB4	ggggacaactttgtatagaaaagttg
		attB1r	ggggactgctttttttgtacaaacttgg
		attB2r	ggggacagctttcttgtacaaagtgggt
		attB3	ggggacaactttgtataataaagttgg
The mRuby2 fluorescent protein gene	Cloning mRuby2 FP gene into pDONR-P2rP3	Fw	attB2r-atggtgtctaagggcgaaga
		Rv	attB3-ttacttgtacagctcgtccatcc
The Clover fluorescent protein gene	Cloning Clover FP gene into pDONR-P2rP3	Fw	attB2r-atggtgagcaagggcgag
		Rv	attB3-ttacttgtacagctcgtcca

Movie S1 (separate file). Combined time-lapse (1-min interval) live cell image movie (15 mins in total) of inward F-actin movement visualized by *proFWA::Lifeact:Venus* in the Arabidopsis central cell of the mock, 10 μM wiskostatin application, *scar2-1*, 200 μM CK-666 application, *arp2-1*, *scar4-1*, *scar2-1*;*scar4-1*, *dis2-1* and *arpc4-t2* (related to figure 1 and supplementary figure 1). Scale bar = 20 μm.

Movie S2 (separate file). Combined time-lapse (1-min interval) live-cell image movie (15 mins in total) of F-actin inward movement visualized by *proFWA::Lifeact:Venus* in the Arabidopsis central cell of the mock, 20 mM BDM application, 50 mM BDM application, and the *xi-g* mutant background (related to figure 3). Scale bar = 20 μm.

Movie S3 (separate file). Combined time-lapse (5-sec interval) live-cell image movie (5 mins in total) of mitochondrial movement visualized by *proDD65::coxIV:GFP* in the Arabidopsis central cell of the mock, 20 mM BDM application, 50 mM BDM application, *xi-g*, *arp2-1* and *scar2-1* mutants (related to figure 4 and supplementary figure 5). Scale bar = 20 μm.

Movie S4 (separate file). Time-lapse (20-sec interval) live-cell image movie (15 min in total) of *in vitro* fusion of the tobacco sperm nucleus with the central cell nucleus. (related to figure S3).

SI References

1. M. Sun, H. Yang, C. Zhou, Single-Pair Fusion of Various Combinations Between Female Gametoplasts and Other Protoplasts in Nicotiana tabacum. *Chin. Sci. Abstr. Ser. B* **2 Part B**, 36 (1995).

2. X. Peng, T. Yan, M. Sun, The WASP-Arp2/3 complex signal cascade is involved in actin-dependent sperm nuclei migration during double fertilization in tobacco and maize. *Sci. Rep.* **7**, 43161 (2017).

3. K. Gooh, *et al.*, Live-Cell Imaging and Optical Manipulation of Arabidopsis Early Embryogenesis. *Dev. Cell* **34**, 242–251 (2015).

4. J. Schindelin, *et al.*, Fiji: an open-source platform for biological-image analysis. *Nat. Methods* **9**, 676–682 (2012).

5. K. Iwabuchi, R. Minamino, S. Takagi, Actin Reorganization Underlies Phototropin-Dependent Positioning of Nuclei in Arabidopsis Leaf Cells. *Plant Physiol.* **152**, 1309–1319 (2010).

6. Y. Zhang, *et al.*, A Highly Efficient Agrobacterium-Mediated Method for Transient Gene Expression and Functional Studies in Multiple Plant Species. *Plant Commun.* **1**, 100028 (2020).

7. S. Li, L. Blanchoin, Z. Yang, E. M. Lord, The Putative Arabidopsis Arp2/3 Complex Controls Leaf Cell Morphogenesis. *Plant Physiol.* **132**, 2034 (2003).